

# Particle-Initiated Breakdown in Gas-Insulated Co-axial Configuration

M. M. El Bahy, S. A. Ward, R. Morsi and M. Badawi  
Faculty of Engineering, Benha University, Cairo, Egypt

**Abstract-** This paper presents theoretical investigation of conducting particle-initiated breakdown in gas-insulated co-axial configuration under high direct voltage. The presence of contaminating conducting particles could seriously deteriorate the dielectric strength of high voltage gas-insulated substations (GIS) and gas-insulated transmission lines (GITL). This deterioration depends on the shape of the particle, the type and the pressure of the gas insulation, and the electric field. The calculated breakdown voltage initiated by particle is obtained by streamer breakdown criterion. The breakdown voltage calculation calls first for an accurate calculation of the electric field on and around the particle surface. The investigated gap is a three-dimensional field problem due to the asymmetrical space arrangement of the particle inside the gap. The particles studied are of many different shapes and sizes such as spheres, filamentary (wire) particles and fine spheres simulating the surface roughness. To solve this problem, charge simulation technique is used. The calculated field values are utilized in evaluating the breakdown voltage. The effects of varying the field nonuniformity, particle shape and size, gas type and pressure on the breakdown voltage are investigated. The calculated breakdown voltage values agree satisfactorily with those measured experimentally and with those obtained theoretically before.

## I. INTRODUCTION

The breakdown voltage of compressed GIS and GITL has been known to drop severely due to the presence of contaminating conducting particles. Many studies were carried out to determine the role of these particles in initiating breakdown [1-6]. The particles may be free to move under the influence of the applied field or may be fixed on the coaxial cylinders in the form of a protrusion representing surface roughness. When they are present and are in contact with inner or outer cylinder, they acquire a charge, depending on the applied field and its size. At a particular field it will be lifted and will be moved towards the opposite cylinder. Before reaching the lifting field, the field at the particle may be sufficient to initiate breakdown.

In this paper, theoretical investigation of conducting particle-initiated breakdown in gas-insulated co-axial configuration under high direct voltage is presented. This configuration has been used for simulating the structure of GIS and GITL. The effect of particle size and shape for both SF<sub>6</sub> and air at pressures up to 15 atm in a plain co-axial gap is presented. The particles studied in this paper are placed in contact with the cylinders and are of different shapes and sizes such as spheres, filamentary (wires) and fine spheres simulating the surface roughness. The wire particle is represented by a cylinder, hemispherically terminated at

both ends, and is placed longitudinally touching one of the co-axial cylinders. Breakdown voltage calculation is based on the assumption that breakdown takes place whenever the primary avalanche attains a critical size; i.e. by the streamer formation criterion [7,8]. This calls first for an accurate calculation of the electric field on and around the particle surface. The field calculation is based on the accurate charge simulation technique (CST) [6, 9-11]. The calculated field values agree well with those values obtained theoretically before. Then, the field values are utilized for calculating the breakdown voltage. The calculated breakdown values agree satisfactorily with those measured experimentally and with values obtained theoretically before.

## II. METHOD OF ANALYSIS

### A. Breakdown Criterion

Electrical breakdown of a gas occurs when sufficient free charges are present to form a conducting plasma channel that bridges the gap. Electron multiplication or avalanche is a source of free charges. An electron avalanche will develop in electronegative gases when the Townsend ionization coefficient ( $\alpha$ ) exceeds the electron attachment coefficient ( $\eta$ ). The transition from an avalanche to a self sustaining discharge can result from streamer formation that occurs when a sufficient charge density accumulates in the gas. These charges alter the local electric field, enhancing the charge multiplication process so that a conducting plasma channel is created by a single avalanche. The critical amount of charge necessary to transform an avalanche to a streamer, is believed to be relatively independent of gas type or pressure and is of the order of 10<sup>8</sup> electrons [7,8]; the conditions for streamer formation are thus fulfilled if:

$$\int_0^{\xi_c} (\alpha(\xi) - \eta(\xi)) d\xi = K \quad (1)$$

Where,  $K$  is a constant, =18 [8] or 10.5 [6,12] for SF<sub>6</sub> in nonuniform and quasi-uniform fields, respectively, and  $\xi_c$  is the critical avalanche length at which  $\alpha(\xi)=\eta(\xi)$ , these coefficients are reported before for SF<sub>6</sub> [12] and air [13].

### B. Electric Field Calculation on and around The Particle Surface

The analysis is based on CST in which the distributed surface charge on each surface of the particle and the inner cylinder is replaced by a set of fictitious simulation charges arranged inside each of them, wherever, the distributed surface charge on the outer cylinder is replaced by another set of charges arranged behind its surface. The satisfaction

of the pertinent boundary conditions results in a set of equations whose simultaneous solution determines the unknown simulation charges. Knowing the simulating charges, the electric potential and field can be calculated at any point on and around the particle surface in the investigated gap [6, 9-11].

1) *Simulation Technique:* The analysis is based on CST [6, 9-11] in which the distributed charge on each surface of inner and outer cylinder is replaced by a set of  $n$  discrete infinite line charges arranged axially inside and behind their surfaces respectively, Fig.1. Each infinite line charge is divided into infinite number of finite line charges. However, instead of each infinite line charge, a definite number  $k$  of finite line charges is considered according to accuracy level. Hence, the number of simulation charges for each cylinder is  $n$  times  $k$  charges.

The distributed charge on the surface of spherical or wire particle is replaced by  $m_1$  point charges and a set of  $m_2$  ring charges arranged inside it, Fig.1. Due to the asymmetrical space arrangement, the ring charges have no constant charge density above their entire perimeter. It can, however, be assumed that the charge density remains constant within a certain angular range, which is determined according to accuracy level. So, each simulating ring charge consists of  $m_3$  ring segments with constant charge density ( $\rho$ ) within a certain angular range, Fig.2. Hence, the number of simulation charges for the particle is  $[m_1+(m_2 \times m_3)]$ . Hence, the total number of simulation charges is  $N=(2 \times n \times k) + m_1 + (m_2 \times m_3)$ .

2) *Coordinates of Simulating Charges:* Fig. 1, shows a cross section of the coaxial gap with a spherical particle placed in contact with the inner cylinder. Inside this cylinder a simulating  $n$  infinite line charges are arranged uniformly at a radius of  $(f_1 \times r)$ . Behind the outer cylinder, a simulating  $n$  infinite line charges are also arranged uniformly at a radius of  $R_o = R + (f_2 \times r)$ .

The charge over the spherical particle is simulated by  $m_1$  points, ( $m_1=2$ ) and  $m_2$  rings arranged inside the particle. The location of the two point charges distant  $\pm (f_3 \times r_s)$  from the particle centre at z-axis. The first ring charge (i.e.  $j_3=1$ ) is placed at a distance of  $z_1=(f_4 \times r_s)$ , from the touch point; while the other rings are arranged according to the relation  $z_{j_3}=[z_1 + f_5 \times (j_3 - 1) \times z_1]$ , and as shown in Fig. 2, the radius of ring charge is a fraction  $f_6$  of particle radius  $r_{oj}$  at the same z-level;  $r_{j_3}=(f_6 \times r_{oj})$  and each ring charge is divided into  $m_3$  segment ring charges with constant charge density.

The charge over the wire particle is simulated by  $m_1$  points, ( $m_1=2$ ) and  $m_2$  rings arranged inside the particle. For the cylindrical part, the surface charge is simulated by uniformly distributed  $m_4$  rings that vary in number depending on its length ( $\ell_w$ ) to its radius ( $r_w$ ) ratio ( $\ell_w/r_w$ ),  $m_4$  equals  $[f_7 \times (\ell_w/r_w)]$ . For each hemispherical tip, the surface charge is simulated by a point charge placed at a distance ( $f_8 \times r_w$ ) from the tip center and two ring charges arranged

uniformly inside each tip. Hence, the total number of simulation charges inside wire particle is  $(m_1+m_2)$ ,  $m_2=(4+m_4)$ .

The problem is now reduced to the determination of the optimum values of integers  $n, k, m_1, m_2, m_3, m_4$  and factors  $f_1$  to  $f_8$ .

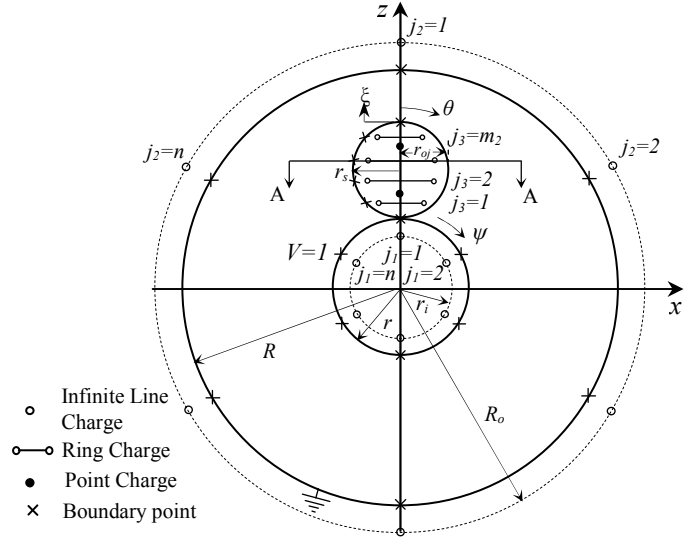


Fig. 1 Discrete simulation charges and boundary points in a cross section of coaxial cylinder gap with a spherical particle in contact with inner cylinder

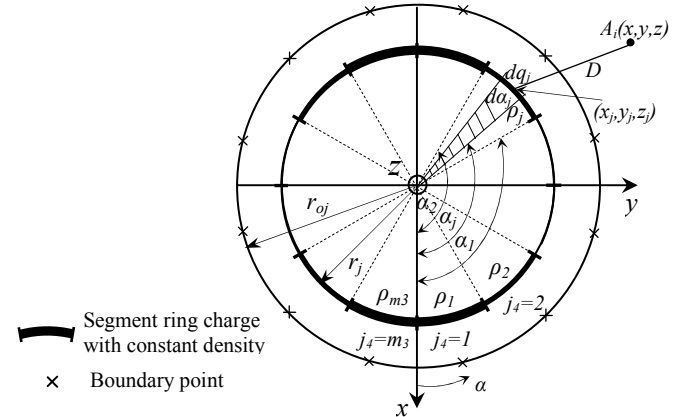


Fig. 2 Discrete simulation ring charge, divided into equal segment ring charges with constant charge density, placed at section A-A in Fig.1.

3) *Coordinates of Boundary Points:* To satisfy the boundary conditions, a boundary point, corresponding to each simulation charge, is chosen along the coaxial cylinders and around the particle surface, Figs. (1,2). Hence, the number of boundary points equals the number of simulation charges ( $N$ ). The boundary points corresponding to the simulation finite line and segment ring charges were chosen midway along the line and segment charges at the cylinders and particle surfaces, respectively. Also, for the simulation point charges, boundary points were chosen at the particle tip and at the touch points.

4) *Potential Calculation*: the potential ( $\phi_i$ ) at an arbitrary boundary point  $A_i(x,y,z)$  is linearly related to all simulation charges by:

$$\phi_i = \sum_{j=1}^{j=N} p_{i,j} q_j \quad (2)$$

where,  $p_{i,j}$  is the potential coefficient of the  $i^{\text{th}}$  boundary point relative to simulation charge  $q_j$ ;  $p_{ij}$  is defined in [9], [10] for point charges, finite line and segment ring charges, respectively.

5) *Electric Field Calculation*: It is well known that the electric field intensity ( $E$ ), is the negative gradient of the potential ( $\phi$ ). It is given, at an arbitrary point  $A_i(x,y,z)$ , by the vector sum of the individual components contributed by the known simulation charges (points, finite lines and ring segments). Hence, the field intensity components  $Ex_i$ ,  $Ey_i$  and  $Ez_i$  at point  $A_i(x,y,z)$  are obtained as follows:

$$Ex_i = \sum_{j=1}^{j=N} Ex_{i,j}, \quad Ey_i = \sum_{j=1}^{j=N} Ey_{i,j}, \quad Ez_i = \sum_{j=1}^{j=N} Ez_{i,j} \quad (3)$$

Then, the field intensity at that point is calculated by

$$E_i = \sqrt{Ex_i^2 + Ey_i^2 + Ez_i^2} \quad (4)$$

### III. RESULTS AND DISCUSSION

To check the accuracy, check points were chosen midway between the boundary points on the surfaces of the particle and coaxial cylinders. The potential and the field deviation angle errors at these points were assessed to check how well the boundary conditions are satisfied. This check of accuracy was made for (i) a wide range of  $R$  to  $r$  ratio (1.5 – 500), (ii)  $r_s$  to  $r$  ratio (0.0001–0.25), (iii)  $r_w$  to  $r$  ratio (0.005–0.25), the wire shape factor; its length ( $l$ ) to its radius ( $r_w$ ) ratio (2.2–20; unless the length of the particle covers most of the gap length). The accuracy remained the same for these investigated ranges.

The accuracy of a simulation depends strongly on the assumptions concerned with the choice of the number and the coordinates of the simulation charges. The optimum values of factors  $f_1$  to  $f_8$  are  $f_1=0.1$ ,  $f_2=5$ ,  $f_3=0.015$ ,  $f_4=0.12$ ,  $f_5=0.045$ ,  $f_6=0.55$ ,  $f_7=7$  and  $f_8=0.5$ . The number of charges was found to be: (i) for coaxial cylinders  $n=6$ ,  $k=100$ , (ii) for spherical particle  $m_1=2$ ,  $m_2=12$ ,  $m_3=30$ , (iii) for wire particle  $m_1=2$ ,  $m_2=4+m_4$ ,  $m_4=2-126$  for  $(l/r_w)=2.2$  to 20,  $m_3=60$ . Hence, the total number of simulation charges ( $N$ ) for spherical particle is 1562 and  $N$  for wire particle varies from 1562 to 9002 for the two limits of the wire shape factor.

Fig. 3, 4 show the variation of percent potential and field deviation angle errors around the spherical particle surface which is placed at inner cylinder,  $\alpha$ ,  $\theta$  start from  $0^\circ$  to  $360^\circ$ ,  $0^\circ$  to  $105^\circ$ , respectively. The maximum potential error is  $1.2 \times 10^{-3}\%$ . Over most of the particle surface, (except the narrow zone that lies near the touch point as reported before in [11] over the stranded conductor surface), the maximum field deviation angle error is  $2.7^\circ$ , while, the corresponding

error values are  $1.6 \times 10^{-3}\%$  and  $0.25^\circ$ , respectively, when the particle is placed at the outer cylinder.

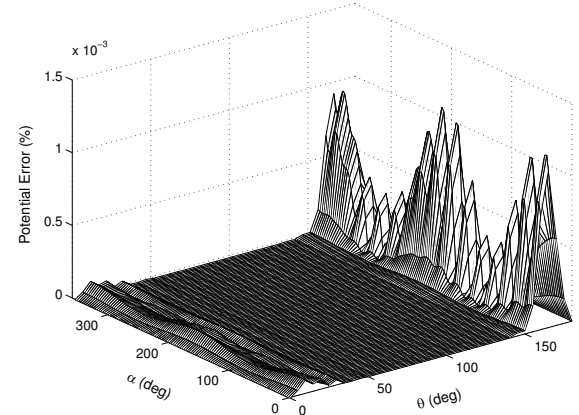


Fig. 3 Variation of percent potential errors around the spherical particle surface lying at inner cylinder, ( $r_s=0.1$ ,  $r=1$ ,  $R=10$ ).

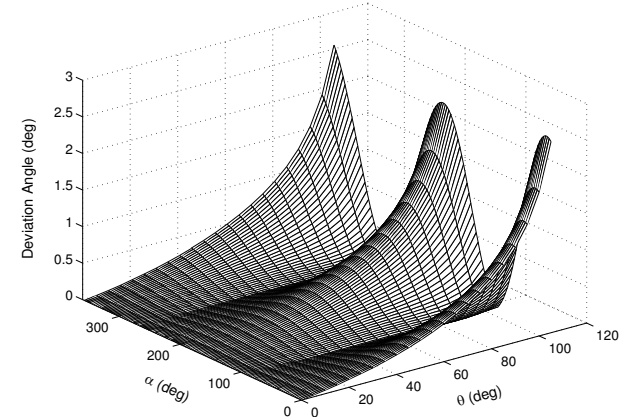


Fig. 4 Variation of deviation angle errors of field around the spherical particle surface lying at inner cylinder, ( $r_s=0.1$ ,  $r=1$ ,  $R=10$ ).

Fig. 5 to 8 show the variation of percent potential and field deviation angle errors around the wire particle surface which placed at inner cylinder for  $r_w=0.1$ ,  $l=0.6$ .

Fig. 5, 6 show the variation of errors around the hemispherical tip,  $\alpha$ ,  $\theta$  start from  $0^\circ$  to  $360^\circ$ ,  $0^\circ$  to  $90^\circ$ , respectively. The maximum errors are 0.045%, and  $1.5^\circ$ .

Fig. 7, 8 show the variation of errors around the cylindrical part; the maximum errors are  $4 \times 10^{-4}\%$  and  $1.7^\circ$  respectively, where  $\beta_w$  is the normalized distance from its tip centre. If the wire particle is placed in contact with the outer cylinder, the maximum errors are ( $8 \times 10^{-3}\%$ ,  $1.6^\circ$ ), ( $3 \times 10^{-5}\%$ , and  $2.2^\circ$ ) for the hemispherical tip and the cylindrical part, respectively.

Along the surface of the coaxial cylinders, the percent potential and field deviation angle errors were calculated and were found to be acceptable over a length of 100 times the inner electrode radius  $r$ .

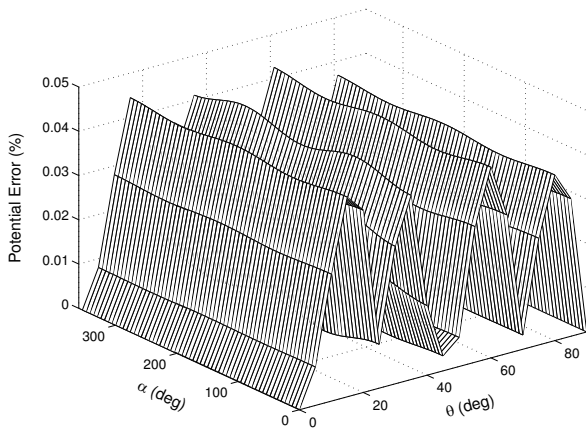


Fig. 5 Variation of percent potential errors around the hemispherical tip of the wire particle ( $r_w = 0.1, l = 0.6$ ) lying at inner cylinder ( $r=1, R=10$ ).

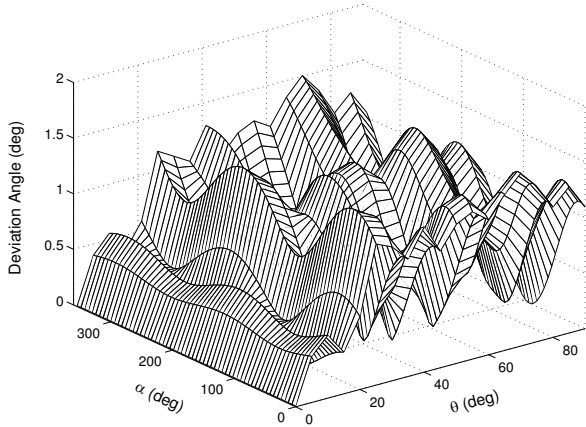


Fig. 6 Variation of deviation angle errors of field around the hemispherical tip of the wire particle ( $r_w = 0.1, l = 0.6$ ) lying at inner cylinder ( $r=1, R=10$ ).

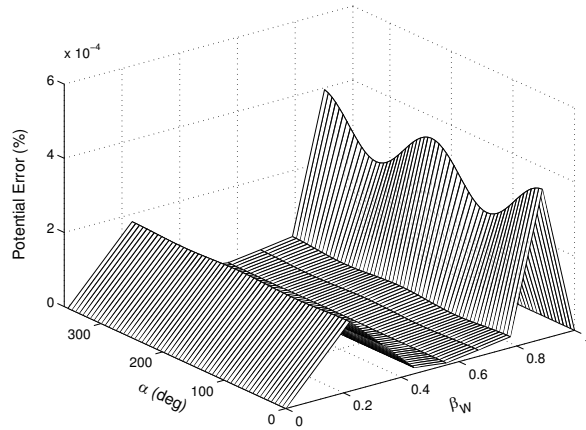


Fig. 7 Variation of percent potential errors around the cylindrical part of the wire particle ( $r_w = 0.1, l = 0.6$ ) lying at inner cylinder, ( $r=1, R=10$ ); where,  $\beta_w$  is the normalized distance over its surface from the tip centre.

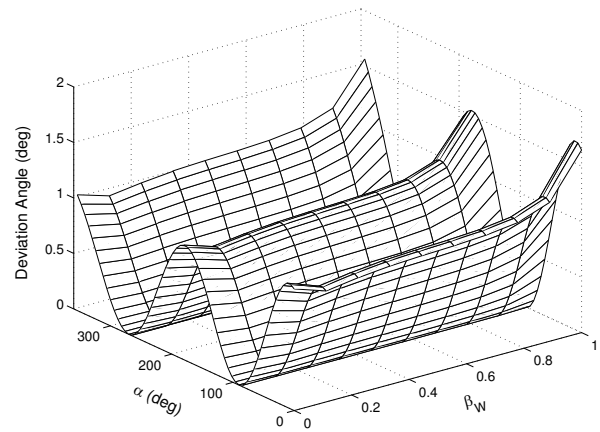
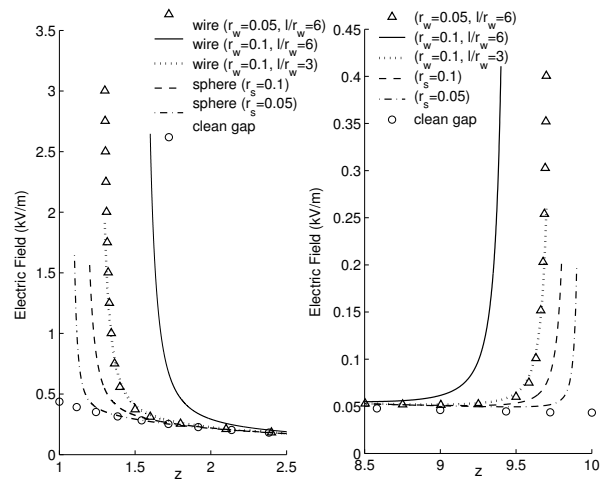


Fig. 8 Variation of deviation angle errors of field around the cylindrical part of the wire particle ( $r_w=0.1, l=0.6$ ) lying at inner cylinder, ( $r=1, R=10$ ).

Fig. 9-(a) and (b) show the electric field distribution in a coaxial gap in the presence of spherical or wire particle located at inner or outer cylinder against the values obtained at clean gap ( $r_s=0.05, 0.1, r_w=0.05, 0.1$  and  $l=0.3, 0.6$ ). The maximum field value depends on the particle shape and size. Both of the wire length and diameter affect greatly this value but variation in spherical particle diameter does not clearly affect this value. As shown in figure, the presence of particles on inner cylinder is more severe than their presence on the outer one.



(a) particle placed at inner cylinder (b) particle placed at outer cylinder  
Fig. 9 Electric Field distribution in a coaxial cylinder gap in presence of a spherical and wire particles ( $r=1, R=10$ ).

Fig. 10, shows a comparison between present and previous [5] calculations of the electric field distribution in an optimized coaxial gap, (where,  $\ln \left[ \frac{R}{r} \right] \approx 1$ ), in the presence of a spherical particle at outer cylinder. The comparison shows excellent agreement between the calculated field values.

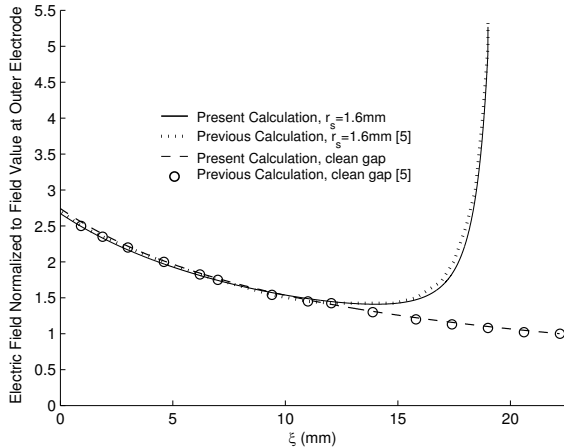


Fig. 10 Electric Field distribution in coaxial cylinder in presence of spherical particle ( $r_s=1.6$ mm) at outer cylinder, ( $r=12.7$ mm,  $R=34.9$ mm).

The field intensification factor at the particle surface tip is responsible for the development of discharge. This factor is defined as the maximum field strength at the particle tip divided by the maximum field strength of the clean gap. When varying the size of spherical particle ( $r_s/r=0.01$  to  $0.25$ ), this factor decreases slightly from  $4.05$  to  $3.13$  and increases slightly from  $1.25$  to  $1.5$ , when the particle is placed on the inner and on the outer cylinder, respectively. Also, when the wire shape factor ( $l/r_w$ ) varies from  $2$  to  $10$ , this factor increases clearly from  $4.05$  to  $11.1$ , increases slightly from  $1.34$  to  $3.68$  when the particle is placed on the inner and on the outer cylinder, respectively. Hence, presence of wire particle is more severe than spherical one and this factor is higher when the particle touches the inner cylinder. Then, the presence of particles on inner cylinder is more severe than their presence on the outer one.

When the streamer formation criterion is used to determine the inception of discharge, the avalanche growth is computed in actual space. To demonstrate the impact of this fact on the foregoing results, Fig. 11 is plotted. Three sets of comparative field distributions are shown. (i) In figure, for  $l/r_w=20$ ; ( $3.9/0.195$ ,  $7.8/0.39$ ),  $l/r_w=10$ ; ( $1.95/0.195$ ,  $3.9/0.39$ ), the field intensification factors are  $18.9$ ,  $18.1$  and  $11.3$ ,  $11.1$ , respectively. Although the wires have equal shape factors and hence have nearly equal surface intensification factors, yet the spatial field distributions are different. (ii) Two wires of the same length ( $3.9/0.39$ ,  $3.9/0.195$ ) will vary in surface fields according to their radii. The two spatial field distributions intersect at  $\xi=0.22$  mm. However, the critical avalanche length is usually small in comparison to this distance unless the two radii are very close in value. (iii) The figure clearly demonstrates the influence of the wire length on avalanche growth ( $3.9/0.195$ ,  $3.9/0.39$ ,  $7.8/0.39$ ). Hence, the thicker wire of the same shape factor of wires, the thinner one of wires having the same length and the longer one of wires having the same diameter lead to the threshold of discharge at lower applied voltages. These concepts agree well with the results obtained in [6]; where the wire particle was found free in uniform field.

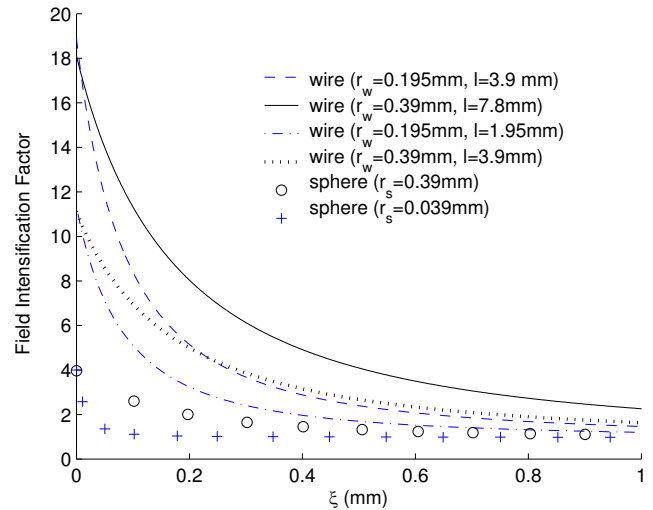


Fig. 11 Field intensification factor of wire and spherical particles lying at inner cylinder ( $r=38$  mm,  $R=125$  mm).

Negative breakdown polarity values are used for comparison as its values are lower than positive polarity values [5]. Fig. 12, shows the calculated and measured negative breakdown voltage in  $SF_6$  and air for a coaxial cylinder gap) in the presence of a spherical and wire particles ( $r_s=0.79$  mm,  $r_w=0.39$  mm,  $l=3.9$  mm) lying at inner cylinder. Breakdown voltage is calculated using streamer criterion; Eq. (1). Breakdown was recorded over  $4.4$  atm, at  $15$  atm, for spherical and wire particles, respectively; i.e. the first streamer developed in the gap was able to propagate across the gap and subsequently initiate a spark (corona-free breakdown occurs). Below these pressure values, the first streamer onset voltage coincides with the onset voltage of corona. The maximum percent error between present calculation and previous measured and calculated values is less than  $10\%$ . The breakdown characteristics of the two kinds of particles are dissimilar; where the critical pressure, which is the border of corona stabilization breakdown zone is larger in case of wire particle presence due to creation of highly nonuniform field.

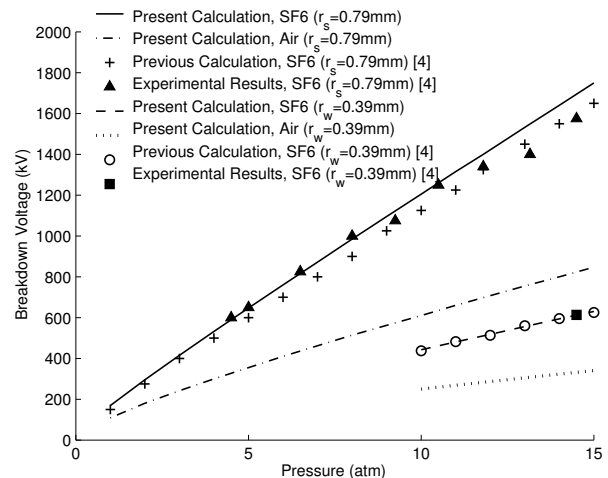
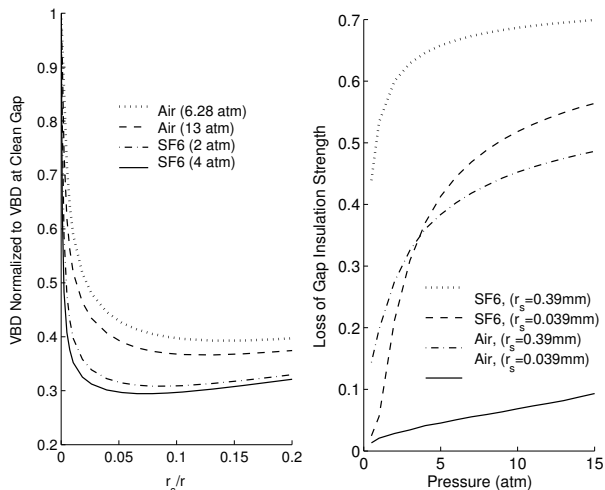


Fig. 12 Calculated and measured negative breakdown voltage for a spherical and wire particles lying at inner cylinder ( $r=38$  mm,  $R=125$  mm).



(a) Normalized breakdown voltage. (b) Loss of gap insulation strength  
Fig. 13 Coaxial cylinder gap in presence of spherical particle at inner cylinder ( $r=38$  mm,  $R=125$  mm).

For pressurized GIS/GITL the corresponding air pressures to SF<sub>6</sub> operating pressures 2 and 4 atm (having the same breakdown voltages) are 6.28 and 13 atm, respectively. Referring to breakdown voltage at clean gap, Fig. 13-a, shows the normalized breakdown voltage of coaxial-cylinder gap versus ( $r_s/r$ ) in pressurized air and SF<sub>6</sub> where the particle is placed at inner cylinder. The figure shows a minimum  $V_{bd}$  value at operating pressures 2, 4 atm was initiated at particle size ratio ( $r_s/r$ )=0.084, 0.074 in SF<sub>6</sub>, respectively. The figure shows also that SF<sub>6</sub> is more sensitive to the presence of fine spherical particles. For practical cylinder finishes, SF<sub>6</sub> at 4 atm retains only half of its potential dielectric strength [14]. The upper limit for the production processes associated with GIS systems equals 35 $\mu$ m (for coaxial gap,  $r=11$ mm,  $R=30$ mm) [15], i.e. ( $r_s/r$ )=0.003. Present calculation gives the normalized  $V_{bd}$  = 0.46, 0.7 and the corresponding loss of gap insulation strength is 0.54, 0.3, for SF<sub>6</sub> and air at 4 and 13 atm, respectively, Fig. 13-b. Hence, the normalized  $V_{bd}$  value of SF<sub>6</sub> agrees well with the value reported before for fine spherical particle simulating the practical cylinder finishes. Then, due to the presence of spherical particle ( $r_s=0.39$  mm) at inner cylinder, the calculated loss of gap insulation strength equals 64%, 48%, for SF<sub>6</sub> and air at 4 and 13 atm respectively. Hence, pressurized air improves the reliability of GIS/GITL in the presence of particles.

#### IV. CONCLUSIONS

1. Three-dimensional electric field is accurately calculated in a co-axial configuration in the presence of spherical, fine spherical simulating surface roughness, wire particles at inner or at outer cylinder using CST.
2. The presence of particles at inner cylinder is more severe than their presence on the outer one.
3. The field distribution depends on the particle shape and particle size. Both of the wire length and diameter affect greatly the maximum value and the distribution

of the field, but varying spherical particle diameter does not greatly affect the maximum value. The thicker wire of the same shape factor wires, the thinner one of wires having the same length and the longer one of wires having the same diameter lead to the inception of discharge at lower applied voltages.

4. The calculated field values agree well with those values obtained theoretically before.
5. SF<sub>6</sub> is very sensitive to field perturbations such as conductor surface roughness; at practical pressures of GITL it retains about 54 %, while air retains about 70 % of their potential dielectric strength for practical cylinder finishes. Hence, pressurized air improves the reliability of GIS/GITL.
6. The breakdown characteristics of the two kinds of particles are dissimilar; the type of breakdown in case of wire particle presence is mostly referred to as corona stabilization breakdown, while in case of spherical particle presence is mostly referred to as streamer formation criterion.
7. The maximum percent error in breakdown values between present calculation and previous measured and calculated values is less than 10 %.

#### REFERENCES

- [1] A. H. Cookson and O. Farish, "Particle initiated breakdown between coaxial electrodes in compressed SF<sub>6</sub>", IEEE Trans. on PAS, vol. 92, pp. 871-876, 1973.
- [2] C. M. Cooke, R. E. Wotton and A. H. Cookson, "Influence of particles on AC and DC electrical performance of gas insulated systems at extra-high-voltage", IEEE Trans. on PAS, vol. 96, No. 3, pp. 768-777, 1977.
- [3] A. H. Cookson, O. Farish and G. M. L. Sommerman, "Effect of conducting particles on AC corona and breakdown in compressed SF<sub>6</sub>", IEEE Trans. on PAS, vol. 94, pp. 1329-1338, 1971.
- [4] C. M. Cooke, "Ionization, electrode surface and discharge in SF<sub>6</sub> at extra-high voltages", IEEE Trans. on PAS, vol. 94, No. 5, pp. 1518-1523, 1975.
- [5] F. A. M. Rizk, C. Masetti, R. P. Comsa, "Particle-initiated breakdown in SF<sub>6</sub> insulated systems under high direct voltage", IEEE Trans. on PAS, vol. 98, No. 3, pp. 825-836, 1979.
- [6] H. Anis and K. D. Srivastava, "Free conducting particles in compressed gas insulation", IEEE Trans. on EI, vol. 16, No. 4, pp. 327-338, 1981.
- [7] H. Raether, "Electron Avalanches and Breakdown in Gases", Washington, Butterworths, 1964.
- [8] A. Pederson, "Criteria for spark breakdown in sulphur hexafluoride", IEEE Trans. on PAS, vol. 89, No.8, pp. 2043-2048, 1970.
- [9] N. H. Malik, "A review of the charge simulation method and its applications", IEEE Trans. on EI, vol. 24, No.1, pp. 3-14, 1989.
- [10] D. Utmischi, "Charge substitution method for three-dimensional high voltage fields", Third International Symposium on High Voltage Engineering, Milan, August 28-31, 1979.
- [11] M. M. El-Bahy, M. Abouelsaad, N. Abdel-Gawad and M. Badawi, "Onset voltage of negative corona on stranded conductors", Journal of Physics D: Applied Physics, vol. 40, no. 10, pp. 3094-3101, 2007.
- [12] M. S. Abou-Seada, Kh. I. M. Ali, "Computation of positive corona threshold for compressed SF<sub>6</sub> in space-charge-stabilized non-uniform fields" IEEE IAS Meeting Toronto, Ontario, Canada, pp. 169-173, 1978.
- [13] A.L. Allen, M. Abdel-Salam, M. Boultejdj, I. Cotton and B. H. Tan, "On the fluctuations in positive glow corona", IET Sci. Meas. Technol., 1, (2), pp. 103-112, 2007.
- [14] S. J. Dale, M. D. Hopkins, "Methods of particle control in SF<sub>6</sub> insulated CGIT systems" IEEE Trans. on PAS, vol. 101, No.6, pp. 1654-1663, 1982.